Temerova, Diana; Chou, Tai Che; Kisel, Kristina S.; Eskelinen, Toni; Kinnunen, Niko; Jänis, Janne; Karttunen, Antti J.; Chou, Pi-Tai; Koshevoy, Igor O.

Hybrid Inorganic-Organic Complexes of Zn, Cd, and Pb with a Cationic Phenanthro-diimine Ligand

Published in:
Inorganic Chemistry

DOI:
10.1021/acs.inorgchem.2c02867

Published: 05/12/2022

Document Version
Publisher's PDF, also known as Version of record

Inorganic Chemistry

pubs.acs.org/IC

Article

Hybrid Inorganic–Organic Complexes of Zn, Cd, and Pb with a Cationic Phenanthro-diimine Ligand

Diana Temerova, Tai-Che Chou, Kristina S. Kisel, Toni Eskelinen, Niko Kinnunen, Janne Jänis, Antti J. Karttunen,* Pi-Tai Chou,* and Igor O. Koshevoy*

Cite This: *Inorg. Chem.* 2022, 61, 19220–19231

Read Online

ACCESS | Metrics & More | Article Recommendations | Supporting Information

ABSTRACT: The phosphonium-decorated phenanthro-imidazolyl pyridine ligand, **LP**$^+$Br, readily reacts with zinc(II) and cadmium(II) bromides to give inorganic–organic zero-dimensional compounds $[\mathbf{LP}^+ZnBr_2]_2[ZnBr_4]$ (**1**) and $[(\mathbf{LP}^+)_2Cd_2Br_4][CdBr_4]$ (**2**), respectively, upon crystallization. These salts are moderately fluorescent in the solid state under ambient conditions (λ_{em} = 458 nm, Φ_{em} = 0.11 for **1**; λ_{em} = 460 nm, Φ_{em} = 0.13 for **2**). Their emission results from spin-allowed electronic transitions localized on the organic component with the negligible effect of $[MBr_4]^{2-}$ and MBr_2 units. Contrary to ionic species **1** and **2**, lead(II) bromide affords a neutral and water-stable complex $[(\mathbf{LP}^+)_2Pb_3Br_8]$ (**3**), showing weak room-temperature phosphorescence arising from spin–orbit coupling due to the heavy atom effect. The emission, which is substantially enhanced for the amorphous sample of **3** (λ_{em} = 575 nm, Φ_{em} = 0.06), is assigned to the intraligand triplet excited state, which is a rare phenomenon among Pb(II) molecular materials.

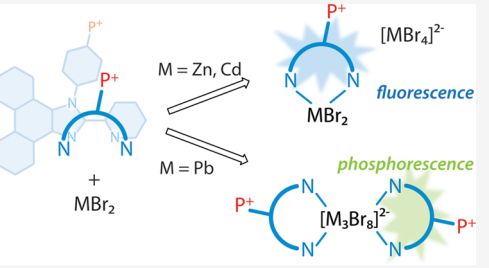

INTRODUCTION

Hybrid materials composed of ionic organic and metal halide components, where metal is a post-transition element from groups 12–15, demonstrate remarkably rich photophysical behavior and have been intensely investigated due to their potential optoelectronic applications, covering electroluminescent devices, solar cells, detectors, and sensors.[1−5] Optical properties of such materials are generally defined by the architecture and composition of halometalate moieties along with characteristics of the lattice, which opens wide possibilities for tuning physical performance once structure–property relationships are understood. In particular, the large variability of organic ionic blocks affects connectivity within an anionic metal halide framework, which can adopt from zero- (0D) to three-dimensional (3D) topology in the crystalline state.[6,7] Utilization of sterically demanding cations typically results in the formation of 0D hybrids, i.e., those comprising individual metal halide anions of mononuclear and cluster nature, spatially separated by organic "insulators".[8−11] Due to relatively nonrigid structural confinement imposed by the lattice, these compounds often exhibit broad photoemission with large Stokes shifts and can reach exceptionally high quantum yields.[10,12−18]

The majority of hybrid systems include nonconjugated organic cations, which play a negligible electronic role and influence photophysics by governing the crystal packing, the subtle structural features, and the local environment of the metal halide anionic components (Scheme 1A). Nevertheless, recently, there has been an increasingly growing number of reports on organic–inorganic compounds, which employ aromatic chromophores as cations having a noticeable or even dominating contribution to the luminescence of such ionic materials (Scheme 1B). Thus, the resonant energy transfer from one-dimensional (1D) lead chloride chains to organic molecules was proposed for broad-band luminescence demonstrated by $[(aminoquinoline)H_2][PbCl_4]$ salt.[19] The prevailing blue-to-white fluorescence originating from quaternized organic bases (various pyridines; pyrimidines; ethylene-, benzyl-, and stilbenyl amines; etc.) is observed for $[MX_3(dmso)]$ (M = Zn, X = Br; M = Cd, X = I),[20] $[ZnX_4]^{2-}$,[13,21,22] $[InBr_4]^-$,[23] $[PbCl_5]^{3-}$,[24] and $[PbCl_3]^-$[25] derivatives, the quantum yields and photostability being substantially higher than those for parent organic halide salts. Alternatively, the related compounds [(aminopyridinium)]-$[HgBr_4]$,[13] [diammoniumdiphenyl sulfone]$[SnCl_6]$,[26] and [bis(pyridinium)propane]$[Pb_2X_6]$[27] display broad-band luminescence due to the interplay of inorganic (self-trapped) and organic-localized excitons.

Optical properties of the inorganic–organic ionic compounds are further broadened by populating the triplet excited states, leading to room-temperature phosphorescence.[3,28] The

Received: August 10, 2022
Published: November 22, 2022

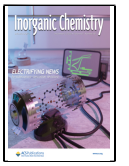

Scheme 1. Illustration of Inorganic−Organic Hybrids Based on Different Types of Organic Cations: (A) Aliphatic Nonemissive Cations; (B) Noncoordinating Cations with Chromophore Groups; and (C) Chromophore Cations with Coordinating Function

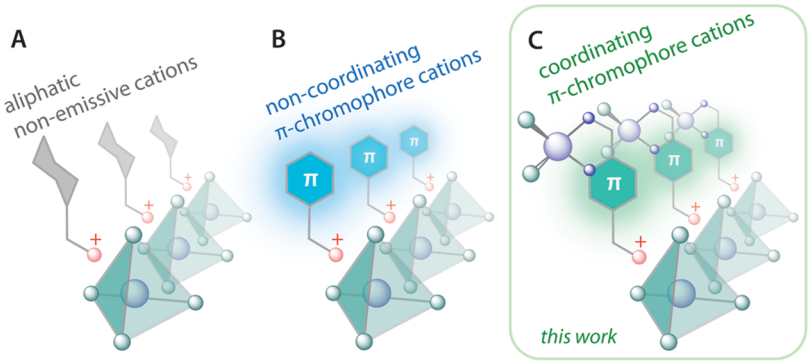

lifetimes and quantum yields of organic ultralong photoemission can be readily modulated by means of the external heavy atom effect, i.e., varying the nature of the constituting halometalates, that was shown for complexes [benzoquinolinium][Pb_2X_5],[29] [PPh_4][ZnX_4],[30] and [PPh_4]-[Cd_2X_6],[31] the latter for X = Br reaches notably high Φ_{em} = 63% (τ = 37.85 ms).

Another approach to diversify the structural organization and photophysical characteristics of hybrid compounds potentially relies on the employment of cationic chromophores with coordinating function and yet remains virtually unexplored (Scheme 1C). The aromatic ligands, e.g., strongly binding N-donors (bi-/tripyridine, phenanthroline, and other heterocycles), decorated with remote positively charged groups (pyridinium/quinolinium, phosphonium, ammonium, etc.) are not exceptional and have been used in the design of a number of phosphorescent complexes of Ru, Re, Ir, and Pt for bioimaging applications,[32] and some Cu(I) zwitterionic iodide clusters with delayed fluorescence.[33,34] These sorts of constructing elements, however, have not penetrated the field of inorganic−organic systems built of post-transition metals, except sporadic examples like [(quinolinium terpyridine)-$ZnBr_2$][$ZnBr_4$(dmso)],[35] confirming the preparative feasibility of the given strategy.

From the photophysical viewpoint, it is well known that group 12 metal halides, which are used as starting reagents for the fabrication of halometalate-based hybrids, and the related salts MX_2 (M = Zn, Cd) readily form fluorescent complexes with chelating N- and O-donors (e.g., N-heterocyclic and Schiff bases, salen-type ligands, etc.) adopting 4-, 5-, and 6-coordination numbers.[36−45] Coordination of the metal centers may lead to the conformational modification[46] and substantial perturbation of the electronic structure of organic molecules, resulting in, e.g., enhanced intramolecular charge transfer,[39,40,47] appearance of stimuli-responsive and sensing ability,[40,43−45,48,49] suppression of photoinduced electron transfer, and dramatic improvement of quantum efficiency typically accompanied by the bathochromic shift of the emission.[36,39,46,47,50] On the other hand, the coordinated MX_2 units tend to participate in intermolecular noncovalent interactions, which have a strong impact on the solid-state arrangement and the corresponding optical properties.[41,42,51]

In comparison to zinc and cadmium, the coordination chemistry of main group metals is less developed for the soft N-heterocyclic ligands and is illustrated by pseudo-octahedral complexes of Pb(II), forming 1D polymeric chains [Pb(diimine)$(\mu$-X$)_2]_n$,[52−56] the emission energy of which is regulated by aromatic system.[56]

To probe the viability of the concept illustrated in Scheme 1C and to utilize the cationic chromophore ligand in the synthesis of low-dimensional metal hybrids, as a case study, we have chosen easy-to-obtain and -modify phenanthrene fused with the chelating imidazolyl-pyridine motif, which readily coordinates to late transition metals as was earlier shown by us and other groups.[42,57,58] The decoration of this fluorescent diimine ligand with the chemically robust tetraarylphosphonium group affords a bulky metal-binding cation, which was explored in the preparation of hybrid compounds derived from Zn, Cd, and Pb halide units.

EXPERIMENTAL SECTION

General Comments. 1-(4-Bromophenyl)-2-(pyridin-2-yl)-1*H*-phenanthro[9,10-*d*]imidazole (**LBr**) was prepared according to the reported procedure.[58] Other reagents were used as received. Toluene was distilled over Na-benzophenone ketyl under a nitrogen atmosphere prior to use. The solution ^{1}H and ^{31}P{^{1}H} spectra were recorded on a JEOL 500 spectrometer. Microanalyses were carried out in the analytical laboratory of the University of Eastern Finland.

Triphenyl(4-(2-(pyridin-2-yl)-1*H*-phenanthro[9,10-*d*]-imidazol-1-yl)phenyl) Phosphonium Bromide (LP$^+$Br). The synthesis was carried out in a pressure tube following the general protocol for the preparation of tetraarylphosphonium salts.[59] The tube was charged with solid **LBr** (0.5 g, 1.11 mmol), triphenylphosphine (0.291 g, 1.11 mmol), and Pd_2(dba)$_3$ (6.4 mg, 0.007 mmol), which were degassed, and dry toluene (0.7 mL) was added under a nitrogen atmosphere. The reaction mixture was heated to 140 °C for 12 h, resulting in the gradual formation of a precipitate of the phosphonium salt. The suspension was cooled down to room temperature, the solvent was removed by filtration, and the crude product was washed with diethyl ether (2 mL × 5 mL). The solid was dried and further purified by column chromatography (silica gel 70−230 mesh, ⌀4 cm × 15 cm, eluent dichloromethane/methanol 40:1 → 10:1 v/v mixture) to afford a pale creamy amorphous material after evaporation of the volatiles (688 mg, 87%). ^{1}H NMR (acetonitrile-d_3, 298 K; δ): 8.86 (d, J_{HH} 8.0 Hz, 1H), 8.79 (d, J_{HH} 8.0 Hz, 1H), 8.75 (dd, J_{HH} 7.8, 1.2 Hz, 1H), 8.39 (dt, J_{HH} 7.9, 1.0 Hz, 1H), 8.24 (ddd, J_{HH} 4.8, 1.8, 0.9 Hz, 1H), 7.97−7.92 (m, 5H), 7.92−7.86 (m, 3H), 7.82−7.74 (m, 13H), 7.70 (ddd, J_{HH} 8.4, 7.1, 1.5 Hz, 1H), 7.60 (ddd, J_{HH} 8.4, 7.0, 1.3 Hz, 1H), 7.39 (ddd, J_{HH} 8.3, 7.0, 1.2 Hz, 1H), 7.31 (ddd, J_{HH} 7.6, 4.8, 1.2 Hz, 1H), 7.22 (dd, J_{HH} 8.4, 1.0 Hz, 1H). ^{31}P{^{1}H} NMR (acetonitrile-d_3, 298 K; δ): 23.7 (s). ^{1}H NMR (*N*,*N*-dimethylformamide-d_7, 298 K; δ): 9.01 (d, J_{HH} 8.2 Hz, 1H), 8.95 (d, J_{HH} 8.4 Hz, 1H), 8.80 (dd, J_{HH} 8.0, 1.3 Hz, 1H), 8.48 (dt, J_{HH} 7.9, 1.0 Hz, 1H), 8.34 (ddd, J_{HH} 4.8, 1.7, 0.9 Hz, 1H), 8.29−8.25 (m, 2H), 8.20−8.14 (m, 2H), 8.10−7.94 (m, 15H), 7.88−7.81 (m, 2H), 7.75

https://doi.org/10.1021/acs.inorgchem.2c02867
Inorg. Chem. 2022, 61, 19220−19231

Scheme 2. Synthesis of the Cationic Diimine Ligand and Its Zn, Cd, and Pb Complexes

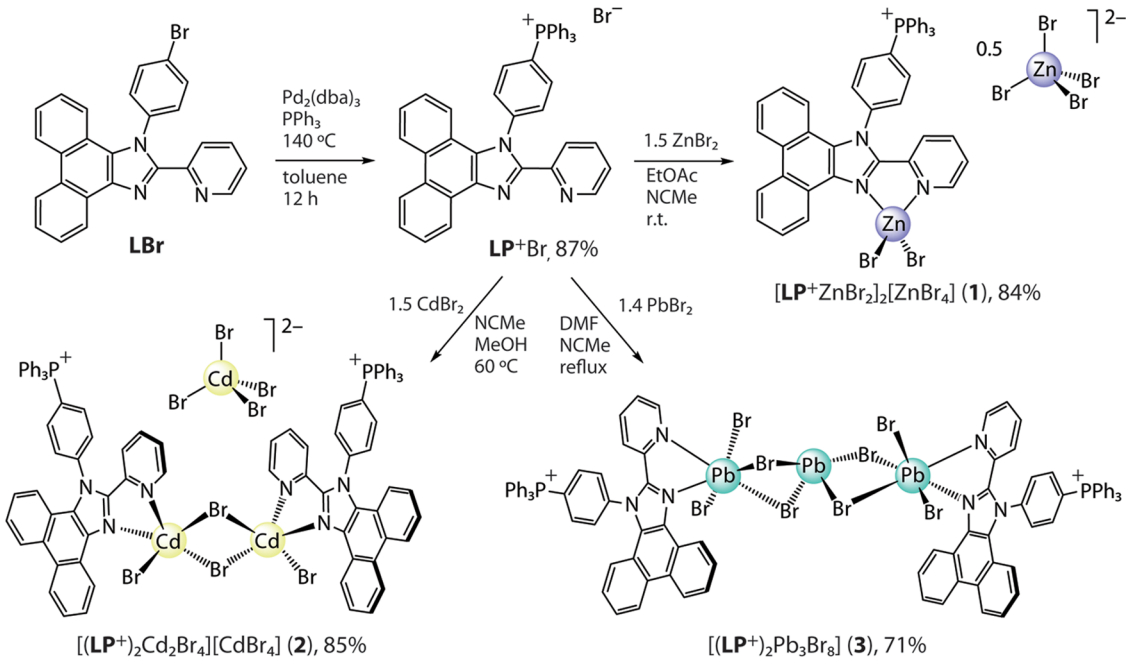

(ddd, J_{HH} 8.4, 7.0, 1.5 Hz, 1H), 7.64 (ddd, J_{HH} 8.3, 7.0, 1.2 Hz, 1H), 7.45−7.38 (m, 2H), 7.28 (dd, J_{HH} 8.3, 1.0 Hz, 1H). ESI-MS (m/z): $[M]^+$ 623.2267 (calcd 623.2256). Anal calcd for $C_{44}H_{31}BrN_3P$: C, 74.16; H, 4.38; N, 5.90. Found: C, 73.84; H, 4.69; N, 5.82.

$[LP^+ZnBr_2]_2[ZnBr_4]$ (1). A solution of $ZnBr_2$ (47 mg, 0.21 mmol) in ethyl acetate (5 mL) was added to a solution of **LP**$^+$Br (100 mg, 0.14 mmol) in acetonitrile (20 mL). The reaction mixture was stirred for 30 min, and a nearly transparent solution was filtered and left at room temperature for slow evaporation to give a white crystalline material (124 mg, 84%). ^{1}H NMR (acetonitrile-d_3, 1.69×10^{-3} M, 298 K; δ): δ 8.93 (d br, J_{HH} 7.8 Hz, 1H), 8.90 (d, J_{HH} 8.3 Hz, 1H), 8.85 (d, J_{HH} 8.3 Hz, 1H), 8.70 (s br, 1H), 8.19−8.05 (m, 4H), 8.00−7.93 (m, 4H), 7.88−7.77 (m, 15H), 7.70−7.64 (m, 2H), 7.43 (ddd, J_{HH} 8.2, 7.1, 1.0 Hz, 1H), 7.05 (d, J_{HH} 7.4 Hz, 1H). ^{31}P{^{1}H} NMR (acetonitrile-d, 298 K; δ): 23.8 (s). Anal calcd for $C_{88}H_{62}Br_8N_6P_2Zn_3 \cdot CH_3CN$: C, 50.47; H, 3.06; N, 4.58. Found: C, 50.63; H, 3.11; N, 4.76.

$[(LP^+)_2Cd_2Br_4][CdBr_4]$ (2). $CdBr_2$ (42 mg, 0.15 mmol) and **LP**$^+$Br (71 mg, 0.10 mmol) were suspended in a mixture of acetonitrile (12 mL) and methanol (6 mL). The suspension was heated at ca 60 °C under stirring until complete dissolution of the solids (ca 15 min). The resulting solution was filtered and concentrated by slow evaporation at room temperature to give a white crystalline material (**2**), which was washed with acetonitrile (5 mL) and diethyl ether (2 mL × 5 mL) and dried (94 mg, 85%). ^{1}H NMR (acetonitrile-d_3, 298 K; δ): 8.89 (d, J_{HH} 6.8 Hz, 1H), 8.85 (d, J_{HH} 8.2 Hz, 1H), 8.79 (dd, J_{HH} 8.1, 1.3 Hz, 1H), 8.69 (s br, 1H), 7.99−7.92 (m, 7H), 7.89 (td, J_{HH} 7.8, 1.7 Hz, 1H), 7.83−7.77 (m, 13H), 7.75−7.69 (m, 2H), 7.63 (ddd, J_{HH} 8.3, 7.1, 1.2 Hz, 1H), 7.53 (dd, J_{HH} 8.7, 3.6 Hz, 1H), 7.38 (ddd, J_{HH} 8.2, 7.1, 1.1 Hz, 1H), 7.09 (d, J_{HH} 8.4 Hz, 1H). ^{31}P{^{1}H} NMR (acetonitrile-d_3, 298 K; δ): 23.8 (s). Anal calcd for $C_{88}H_{62}Br_8Cd_3N_6P_2$: C, 47.15; H, 2.79; N, 3.75. Found: C, 47.08; H, 2.85; N, 3.91.

$[(LP^+)_2Pb_3Br_8]$ (3). A solution of **LP**$^+$Br (70 mg, 0.10 mmol) in acetonitrile (1.5 mL) was added to a solution of $PbBr_2$ (51 mg, 0.14 mmol) in dimethylformamide (3 mL). The resulting mixture was gently refluxed for ca 10 min, giving a nearly transparent pale yellow solution, which was filtered. Gas-phase diffusion of water into this solution at room temperature for 1 week produced **3** as a pale yellow crystalline material, which was washed with acetonitrile (2 mL × 5 mL) and diethyl ether (2 mL × 5 mL) and dried (85 mg, 71%). Anal calcd for $C_{88}H_{62}Br_8N_6P_2Pb_3$: C, 41.84; H, 2.47; N, 3.33. Found: C, 42.04; H, 2.55; N, 3.75.

X-ray Structure Determinations and Powder Measurements. The crystals of **1**−**3** were immersed in cryo-oil, mounted in a Nylon loop, and measured at a temperature of 150 K. The X-ray diffraction data were collected with a Bruker Kappa Apex II diffractometer using Mo Kα (λ = 0.71073 Å) radiation. The APEX2[60] program package was used for cell refinements and data reductions. A numerical or semiempirical absorption correction (SADABS)[61] was applied to all data. The structures were solved by direct methods using the SHELXS-2018[62] program with the WinGX[63] graphical user interface. Structural refinements were carried out using SHELXL-2018.[62]

Some of the crystallization solvent molecules in **2** could not be resolved unambiguously. The acetonitrile solvent molecules were refined with an occupancy of 0.5. The contribution of the missing solvent to the calculated structure factors was taken into account by a SQUEEZE routine[64] of PLATON.[65] The missing solvent was not taken into account in the unit cell content. All non-H atoms were anisotropically refined, and all hydrogen atoms were positioned geometrically and constrained to ride on their respective parent atoms with C−H = 0.95−0.98 Å and U_{iso} = 1.2−1.5U_{equiv} (parent atom). The crystallographic details are summarized in Table S1 (Supporting Information).

Powder X-ray powder diffraction (XRD) patterns were recorded with a Bruker Advance D8 diffractometer using a Cu Kα (1.54184 Å) radiation source (Bruker: 40 kV/ 40 mA). Divergence and receiving slits of 1.0 mm were used together with a Ni filter in the measurements. Prior to measurement, a sample was placed on a Si single-crystal zero background sample holder. The diffraction patterns were scanned from 5 to 90° in a 2θ scale using the locked couple technique in Bragg−Brentano geometry. A collection time of 2 s was used together with a step size of 0.05° per step.

Photophysical Measurements. The excitation and emission spectra for the solid samples were recorded with an Edinburgh FLS980 spectrofluorometer. Photoluminescence quantum yields and the absorption spectra of solid materials were measured by an integrating sphere (F-M01, Edinburgh) set in the sample chamber of the spectrometer (Edinburgh FLS980). Emission lifetimes within 1 ns−20 μs were collected by an inbuilt, time-correlated single photon counting (TCSPC) system (Edinburgh FLS980) coupled with a synchronized diode laser (EPL-375) as the pumping source. For

https://doi.org/10.1021/acs.inorgchem.2c02867
Inorg. Chem. 2022, 61, 19220−19231

phosphorescence lifetimes longer than 50 μs, an intensified charge-coupled detector (PI-MAX ICCD) coupled with a Q-switch laser was used instead. Both timings of ICCD and tunable laser are triggered by a pulse generator (DG-535, Stanford Research System) with signal jittering less than 5 ns. The excitation pulse was generated by an LT-2134 (532 nm, SHG of Nd:Yag laser, LOTIS Tii) followed by an LT-2211 tunable laser (345−532 nm, LOTIS Tii), and 365 nm was chosen as the excitation source with an fwhm of ∼20 ns.

Computational Details. Quantum chemical studies on all complexes were carried out using density functional theory (DFT). The PBE0 hybrid density functional[66,67] in combination with the def2-TZVP basis set[68] and the corresponding scalar-relativistic effective core potential[69] were applied for Cd and Pb atoms. The full model of Cd complex **2** was optimized using a QM/MM approach within the ONIOM framework,[70] since attempts to locate a minimum geometry with the isolated single-molecule model were unsuccessful. In the QM/MM model, the crystal structure was expanded in three dimensions and the central molecule was assigned as the QM part, while the surroundings were kept frozen and treated with MM using the UFF force field.[71] Electronic embedding with the QEq scheme[72] was used to account for polarization of the QM region. The QM/MM optimization was performed using Gaussian 16.[73] All other calculations were performed with Orca 5.0.3[74] using single-molecule models in the optimizations. The geometry of the first excited singlet state was optimized with TD-DFT, while the ground state and first excited triplet state were optimized with DFT. For compound **3**, the implicit CPCM solvation model[75] with toluene as the solvent was used because the geometry optimization did not converge in a vacuum environment. To confirm that the obtained geometries corresponded to a true local minimum on the potential energy surface, frequency calculations were performed for all optimized structures. Furthermore, to study the excitation and emission behavior, single-point TD-DFT calculations were performed for all optimized structures using the range-separated LRC-ωPBEh[76] functional together with the def2-TZVP basis set. The resolution of identity approximation together with the chain of spheres for exchange approximation (RIJCOSX)[77,78] was used in all calculations with Orca to speed up the calculations.

RESULTS AND DISCUSSION

Synthesis and Characterization. The tetraarylphosphonium unit was chosen due to its stability, bulkiness, and accessible synthesis, the conditions of which tolerate the N-heterocycles. Functionalization of the phenanthro-imidazolyl pyridine was performed according to the general method by Marcoux (Scheme 2 and the Supporting Information).[59] The palladium-catalyzed reaction of the bromoaryl precursor (**LBr**)[58] with a stoichiometric amount of triphenylphosphine afforded the corresponding phosphonium bromide (**LP**$^+$Br) in good yield. Hybrid complexes of zinc(II) and cadmium(II) were obtained by treating the $ZnBr_2$ and $CdBr_2$ salts with **LP**$^+$Br in ethyl acetate/acetonitrile and methanol/acetonitrile mixtures, respectively. Slow evaporation of the resulting solutions at room temperature produced colorless crystals of ionic species $[\mathbf{LP}^+ZnBr_2]_2[ZnBr_4]$ (**1**) and $[(\mathbf{LP}^+)_2Cd_2Br_4]$-$[CdBr_4]$ (**2**) suitable for X-ray diffraction analysis. Due to the lower solubility of $PbBr_2$, it was reacted with **LP**$^+$Br in a dimethylformamide/acetonitrile solvent system. Subsequent gas-phase diffusion of water into the reaction mixture gave a neutral complex $[(\mathbf{LP}^+)_2Pb_3Br_8]$ (**3**) as a pale yellow crystalline material (Scheme 2). The formation of **1** and **3** was found to be selective and rather independent of the ratio of starting reagents, while in the case of **2**, proper stoichiometry (**LP**$^+$Br/$CdBr_2$ 2:3) has to be obeyed to minimize crystallization of side products. A slight excess of **LP**$^+$Br in the synthesis of **3** was used to avoid precipitation of $PbBr_2$. The iodide analogues of **1** and **2** can also be obtained in a similar fashion, but the crystalline materials visibly degrade under exposure to light and are virtually nonluminescent under ambient conditions and thus were omitted from this work. In yet another approach, we were unable to prepare the lead iodide complex in a reproducible manner and in pure form.

The structures of **1**−**3** determined by XRD analysis are depicted in Figures 1−3, and selected bond lengths and angles

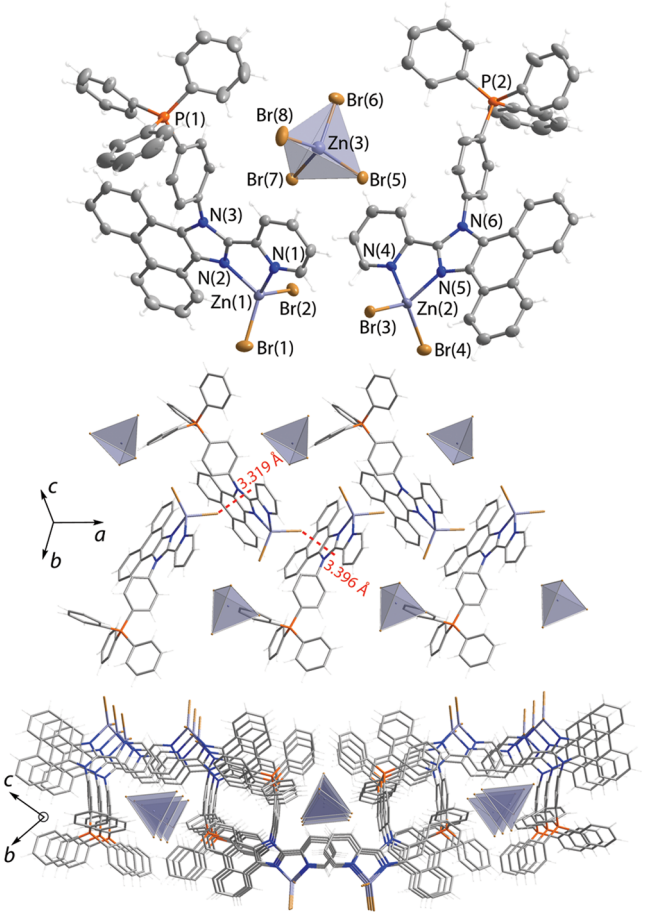

Figure 1. Molecular (top) and packing extended (middle and bottom) structures of salt $[\mathbf{LP}^+ZnBr_2]_2[ZnBr_4]$ (**1**); thermal ellipsoids are shown at 50% probability.

are listed in Table S2 (SI). The repeating motif of salt **1** is composed of individual inorganic dianions $[ZnBr_4]^{2-}$ and two crystallographically nonequivalent metal−organic cations $[\mathbf{LP}^+ZnBr_2]^+$. In turn, the latter constituents comprise the phosphonium-decorated ligand, coordinated to the zinc dibromide unit via chelating imidazolyl-pyridine function. In this cationic complex, the metal center expectedly adopts pseudo-tetrahedral coordination geometry, analogously to the neutral predecessor compounds we described earlier[42] and to other related $[Zn(diimine)Hal_2]$ species.[37,41,46,79]

Cadmium complex **2** reveals the same stoichiometry as that found in **1**, $[\mathbf{LP}^+MBr_2]_2[MBr_4]$, and is topologically similar to the zinc congener (Figure 2). The slightly distorted $[CdBr_4]^{2-}$ tetrahedron is placed in voids formed by tetraarylphosphonium groups, which is apparently driven by the electrostatic attraction. The $[\mathbf{LP}^+CdBr_2]^+$ cations dimerize via the nonsymmetrical bromide bridges (μ_2-Br−Cd distances are 2.640(2), 2614(2), 2.861(2), and 2.802(2) Å; Table S2) that provides

https://doi.org/10.1021/acs.inorgchem.2c02867
Inorg. Chem. 2022, 61, 19220−19231

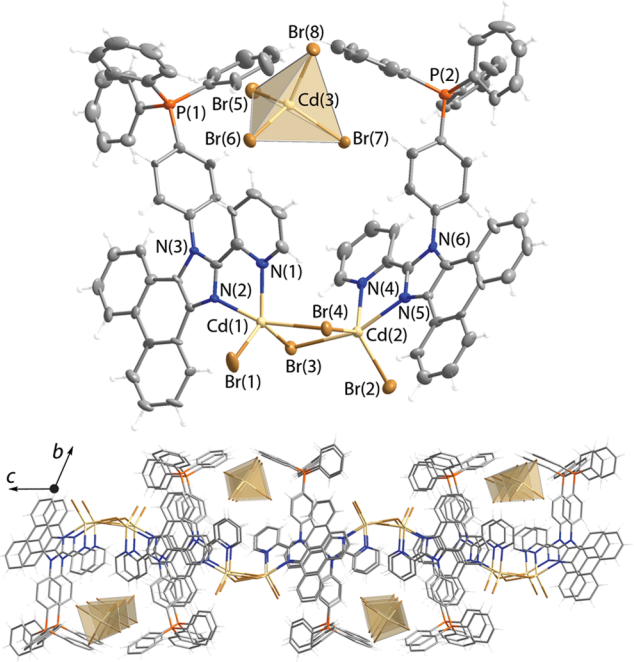

Figure 2. Molecular (top) and packing extended (bottom) structures of salt $[(\mathbf{LP}^{+})_2Cd_2Br_4][CdBr_4]$ (**2**); thermal ellipsoids are shown at 50% probability.

pentacoordinate environment of Cd(II) ions and evidently follows a preference of [Cd(diimine)Hal_2] units to have a higher coordination number than that of Zn(II) analogues.[80−82]

The $[MBr_4]^{2-}$ anions in **1** and **2** form networks of hydrogen bonds with organic molecules and are well separated from each other (Figures 1 and 2); the distances between the bromine atoms of adjacent anions exceed 10 Å (**1**) and 6.6 Å (**2**), which are likely too long for appreciable electronic coupling between these inorganic components.

In contrast to ionic compounds **1** and **2**, lead(II) bromide produced overall neutral molecular entity **3**, which can be seen as a zwitterionic complex built of two cationic ligands coordinated to an anionic bromoplumbate cluster featuring a discrete $[Pb_3Br_8]^{2-}$ core (Figure 3); the complex conceptually resembles the $[Cu_4I_6]^{2+}$ clusters stabilized by $[RP(pyridine)_3]^{+}$ ligands.[33] The anions of the same composition but of somewhat different geometry were found as 1D polymers in salts $[PR_4]_2[Pb_3Br_8]$.[83,84] The trimetallic motif contains a central seesaw $[PbBr_4]^{2-}$ fragment, which is linked to the lateral $PbBr_2$ units via bromide bridges. The geometry of tetracoordinate $[PbBr_4]^{2-}$ is known for ns^2 metal halides[2,9] and is derived from a trigonal bipyramid with a $6s^2$ electron pair of Pb(II) being in the equatorial plane.[85,86] The bond distances from the bridging halides Br(3) and Br(4) to the pendant Pb(1) atom (Br(3/4)−Pb(1) = 3.0893(4) and 3.2068(8) Å) are visibly longer than those within the $[PbBr_4]^{2-}$ block (Br(3/4)−Pb(2) = 2.9932(4) and 2.7250(5) Å). Such deviation of μ_2-Br−Pb separations due to nonsymmetrical coordination has been described for other bromoplumbate clusters.[87,88]

The binding of the $\mathbf{LP}^{+}$ ligand to each of the $PbBr_2$, together with μ_2-bromides, completes the highly distorted octahedral environment of the Pb(1) center. This metal atom lies almost in the plane of the pyridine; the Pb(1)−N_{py}(1) bond length (2.642(3) Å) indicates relatively strong interaction and is

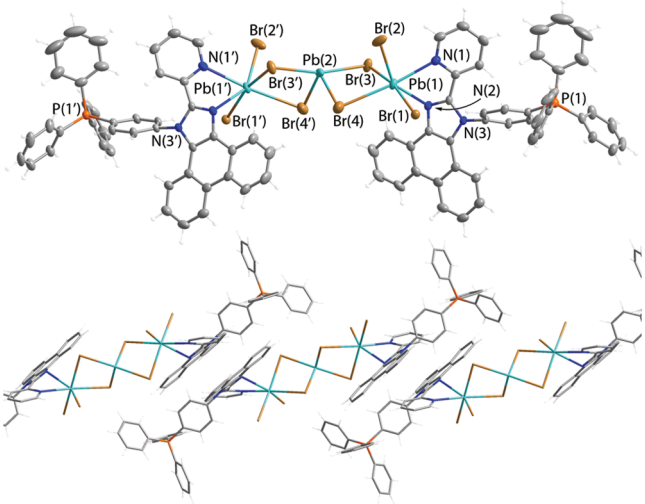

Figure 3. Molecular (top) and packing extended (bottom) structures of complex $[(\mathbf{LP}^{+})_2Pb_3Br_8]$ (**3**); thermal ellipsoids are shown at 50% probability.

consistent with reported data on the Pb(II) diimine halide complexes.[52,54] Bonding of the Pb(1) atom to the diimine function is accompanied by a substantial twisting of the pyridine ring with respect to the imidazole; the corresponding dihedral angle between the planes of these heterocycles equals 33.8° (Figure 3). This might be caused, to a large extent, by intermolecular arrangement, which is probably defined by multiple Br···H contacts (2.73−3.10 Å) due to the Coulombic forces between the bromide ligands and the positively charged tetraarylphosphonium motifs. As a result, the Pb(1) atom is substantially displaced from the plane of imidazole, leading to a longer Pb(1)−N_{imi}(2) distance (2.759(3) Å). This effect can be attributed to the proximity of the lone pair of Pb(II), which causes the elongation and weakening of the Pb−N_{imi} bonding interaction.[89]

The ^{1}H NMR spectra recorded for compounds **1** and **2** in acetonitrile-d_3 at room temperature confirm the presence of complex cations $[\mathbf{LP}^{+}MBr_2]^{+}$ in solution (Figure S1), although broadening of the signals for salt **1** upon dilution suggests some dynamic process. This is likely caused by easy dissociation of MBr_2 units in coordinating solvent and is supported by electrospray ionization (ESI)-mass spectrometry (MS) measurements, which show only the signal of the free ligand. Complex **3** is scarcely soluble in most organic solvents. Its proton spectrum in a dimethylformamide-d_6 solution is identical to that of the free ligand, indicating complete disintegration of the aggregate. Nevertheless, the dissociation does not lead to degradation of the mixture and **3** is efficiently reassembled upon crystallization or slow precipitation with water.

Photophysical Studies and Theoretical Analysis. For the free ligand in a dichloromethane solution, the lowest energy absorption bands (330−360 nm, Figure S2) can be assigned to the predicted $S_0 \rightarrow S_1$ transition (λ = 340 nm) from density functional theory (DFT), which mainly involves charge transfer (ILCT) from imidazole to phosphonium-bearing phenylene and the empty orbital of the P−C bond (Figure S3). The radiative relaxation to the ground state $S_1 \rightarrow S_0$ (λ = 424 nm, Table S3) has virtually identical CT character. In accordance with theoretical results, the observed ILCT fluorescence of $\mathbf{LP}^{+}$Br (λ_{em} = 422 nm, Φ_{em} = 0.1, Figure S2)

https://doi.org/10.1021/acs.inorgchem.2c02867
Inorg. Chem. 2022, 61, 19220−19231

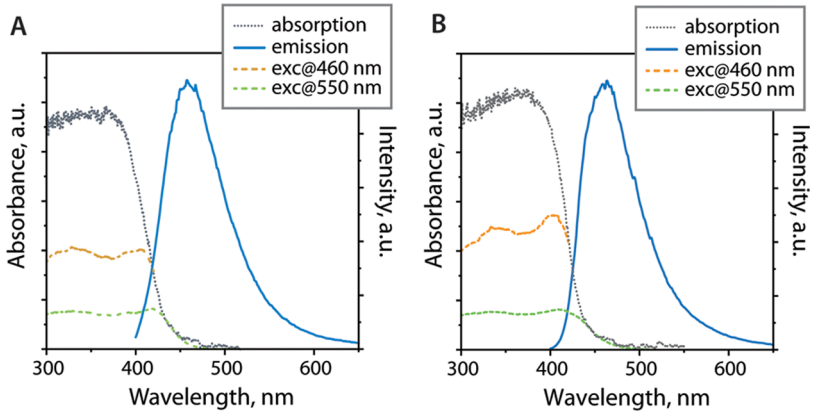

Figure 4. Room-temperature absorption, excitation, and emission (λ_{exc} = 380 nm) spectra of **1** (A) and **2** (B) in the solid state.

Table 1. Photophysical Properties of Compounds 1−3 in the Solid State at 298 K

	λ_{fluo}, nm	τ_{fluo}, ns	λ_{phos}, nm	τ_{phos}, μs	Φ_{em}	k_r,[b] s^{-1}	k_{nr},[b] s^{-1}
LP$^+$Br	456	<1			0.04	>4 × 10^7[c]	>9 × 10^8[c]
1	458	1.3[a]			0.11	8.5 × 10^7	6.8 × 10^8
2	460	1.4[a]			0.13	9.3 × 10^7	6.2 × 10^8
$\mathbf{3}_{cryst}$	440	2.1	517, 550	11	0.009	~8 × 10^2[d]	~9 × 10^4 [d]
$\mathbf{3}_{amorph}$	460	4.0	575	120	0.06	~5 × 10^2[d]	~8 × 10^3[d]

[a]Amplitude-weighted average emission lifetimes for the biexponential decays determined by the equation $\tau_{av} = \sum A_i\tau_i$, A_i = weight of the ith exponent. [b]k_r and k_{nr} were estimated by Φ_{em}/τ and $(1 - \Phi_{em})/\tau$, respectively. [c]Estimated approximately due to the inability to accurately determine the lifetime. [d]Calculated by neglecting the contribution of fluorescence to the value of Φ_{em}.

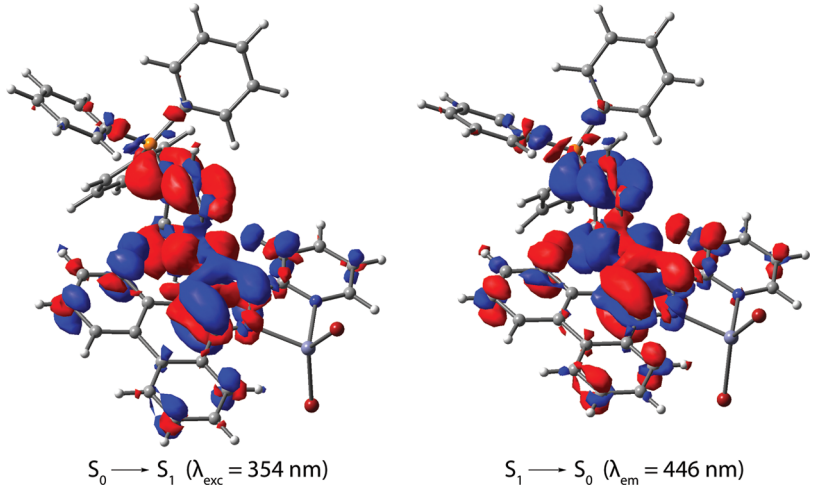

Figure 5. Electron density difference plots for the lowest energy excitation $S_0 \rightarrow S_1$ and emission $S_1 \rightarrow S_0$ in the cation $[\mathbf{LP}^+ZnBr_2]^+$ of compound **1** (isovalue 0.002 a.u., DFT-LRC-ωPBEh method, optimized S_0 and S_1 geometries). During the electronic transition, the electron density increases in the red areas and decreases in the blue areas.

lacks vibronic progression and demonstrates substantial Stokes shift. This behavior markedly differs from that of the neutral analogue **L** (2-pyridyl-1*H*-phenanthro[9,10-*d*]imidazole) with largely phenanthrene-centered structured emission in the UV region (λ_{em} = 370, 388 nm, Φ_{em} = 0.37).[58]

Dried crystals of acetonitrile-solvated **1** and **2** show similar room-temperature luminescence (Figure 4 and Table 1). Both compounds are moderate blue emitters, which exhibit broad and structureless signals maximized at 458 (**1**) and 460 nm (**2**) with quantum yields of 0.11 and 0.13, respectively. The luminescence of the ligand salt **LP**$^+$Br in the solid (λ_{em} = 456 nm, Φ_{em} = 0.04, Figure S2) is substantially weaker, although the peak wavelength is practically unaffected by the presence of the metal units. The average lifetimes (τ_{av} = 1.3 and 1.4 ns) and radiative rate constants ($k_r \approx$ ca 10^8 s^{-1}) point to the singlet origin in the excited state, i.e., fluorescence. A similar enhancement of organic luminescence in the hybrid compounds due to a more rigid environment has been reported for other congener materials.[21,22,24]

Albeit relatively short intermolecular Br$\cdots\pi$ contacts (ca 3.3−3.4 Å, Figure 1) seen in salt **1**, the phosphorescence induced by the external heavy atom effect, which was previously detected for $\mathbf{L}ZnI_2$,[42] cannot be identified in the room-temperature spectra of **1**. The spectroscopic profiles for **1** and **2** resemble those of the complexes $\mathbf{L}ZnX_2$ (X = Cl, I, OAc).[42] Thus, the excitation and emission bands of **1** and **2** are likely associated

https://doi.org/10.1021/acs.inorgchem.2c02867
Inorg. Chem. 2022, 61, 19220−19231

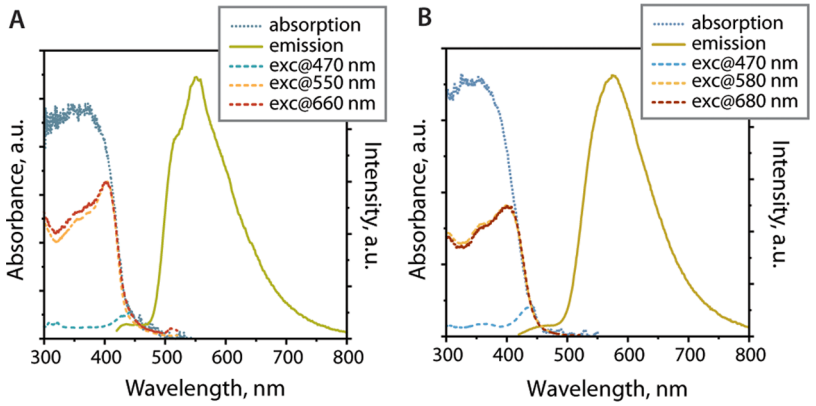

Figure 6. Room-temperature absorption, excitation, and emission (λ_{exc} = 400 nm) spectra of the single crystals (A) and amorphous sample (B) of complex **3**.

with the $[\mathbf{LP}^{+}MBr_2]^{+}$ cations and are dominated by the organic component, whereas the $[MBr_4]^{2-}$ anions do not contribute to the S_1 state. DFT studies of the $[\mathbf{LP}^{+}MBr_2]^{+}$ components (the half model was used for the Cd derivative, Table S3) confirm that the $S_0 \leftrightarrow S_1$ electronic transitions have the same nature as those for the free ligand (Figures 5 and S4) and illustrate the insignificant influence of coordinated MBr_2 units on the optical behavior of **1** and **2**. Compared to the neutral species $\mathbf{L}ZnX_2$, for which the π(phenanthrene) $\rightarrow$ π^*(pyridine) charge transfer was computationally predicted for the low-energy excitation, the appearance of the electron-deficient phosphonium motif decreases the contribution from phenanthrene and pyridine orbitals, substantially changing the character of excitation and emission to π(imidazole) $\leftrightarrow$ π^*(phenylene-P) transitions.

Single crystals of complex **3** are poorly luminescent at room temperature under UV excitation, showing the main low-energy band maximized at 550 nm and a very weak high-energy signal around 440 nm (Figure 6) with a total quantum yield of 9×10^{-3} (Table 1). The latter minor band has a lifetime of 2.1 ns and can be correlated with the intraligand fluorescence of **1** and **2**. The microsecond lifetime of the prevailing band (τ_{obs} = 11 μs) and the corresponding rate constant ($k_r \approx 8 \times 10^2$ s^{-1}) indicate a spin-forbidden process, i.e., phosphorescence. The barely resolved but notwithstanding discernible vibrational structure of the main band points to the triplet state responsible for the emission is localized within the conjugated system of the diimine ligand. This tentative assignment is also implicitly supported by the similarity and broadness of excitation spectra for **1**, **2**, and **3**; for self-trapped exciton emission of zero-dimensional halides, relatively narrow excitation spectra have been typically reported.[13,14,85,88,90]

Remarkably, thorough grinding of single crystals of **3** or vacuum evaporation of a dimethylformamide solution of **3** generates a material with much brighter luminescence. The predominantly amorphous nature of the solid is confirmed by powder XRD measurement (Figure S5). The crystal-to-amorphous phase transition and the decrease of the crystal size do not considerably affect the excitation spectra but red-shift the maxima of both emission bands for ca 20−25 nm, retaining their approximate ratio. This is accompanied by a nearly 7-fold increase in the total intensity (Φ_{em} = 0.06) and the disappearance of the fine structure of the dominating low-energy band. The latter indicates a more significant charge transfer character of the triplet state in the amorphous sample than that in bulk crystals. The gain in quantum yield arises from the suppression of nonradiative decay that is manifested by nearly an order of magnitude drop of the corresponding rate constant for amorphous **3** (Table 1). Despite the fact that the disruption of the lattice is expected to produce a less rigid local environment, the decrease in k_{nr} probably results from the disappearance of intermolecular interactions between organic chromophores (Figure 3), which could quench the luminescence in the neat crystal, making this effect opposite to the one termed "crystallization-induced emission", e.g., in $[PbX_2(4,4'$-bipyridine *N*-oxide$)]_n$ coordination polymers.[91] The switch of weak fluorescence in crystals to stronger phosphorescence in the glass phase was observed for lead(II) alkanoates and explained by the shortening of intermolecular Pb−Pb distances.[92] Importantly, the dominating phosphorescence of amorphous **3** indicates that it is an intrinsic molecular property but not an effect of crystal packing. Furthermore, it confirms an efficient assembly of this complex upon solvent removal, notwithstanding its complete dissociation in solution that opens a way for facile solution processing of these species. In terms of potential practical applications of this sort of compound, the improvement of the photophysical performance in an amorphous state could simplify the fabrication and handling of uniform films for optoelectronic devices.

The presence of a weak prompt fluorescence signal propounds that $S_1 \rightarrow S_0$ radiative relaxation competes with relatively slow intersystem crossing, eventually induced by the heavy atom effect of the lead bromide fragment. The same phenomena were observed in the 77 K spectra for both amorphous **3** and crystalline **3** (Figure S6). Their emission intensities increase significantly by lowering the temperature, which suppresses the thermally induced nonradiative deactivations. For amorphous **3**, its low-temperature fluorescence and phosphorescence bands are blue-shifted ca 20 nm compared to those at room temperature and indicate excited-state destabilization at low temperatures, plausibly due to hindered intermolecular relaxation in the amorphous phase under cryogenic conditions. Support for this viewpoint is given by crystalline **3**, where the intermolecular relaxation is insignificant, and therefore, the fluorescence and phosphorescence peaks remain unchanged by varying the temperature.

Theoretical analysis of **3** was performed using the implicit CPCM solvation model[75] in the DFT calculations because the geometry optimization did not converge in a vacuum environment. The inclusion of toluene as a solvent helped in

https://doi.org/10.1021/acs.inorgchem.2c02867
Inorg. Chem. 2022, 61, 19220−19231

reaching satisfactory optimization of the geometries of S_0 and T_1 states. As the use of solvent is not justified experimentally, because it is absent in the crystal structure of **3**, the character of the predicted $S_0 \rightarrow S_1$ excitation yet remains ambiguous. Given the similarity of the experimental excitation spectra for compounds **1**–**3**, it is reasonable to assume photoinduced IL charge transfer transition (imidazole → phenylene) for **3** as well. The T_1 state for **3** seems to be mostly insensitive to the choice of solvent, and the $T_1 \rightarrow S_0$ emission is governed by the electronic transitions of one of the diimine ligands, which occur within the imidazole ring and the nearest bonds around it (Figure 7). The calculated wavelength for the phosphorescence of **3** (λ_{calc} = 557 nm, Table S3) matches well the observed ones. Regarding the intraligand triplet emission of **3**, it is worth mentioning that such behavior is rare among lead compounds. Long-lived organic phosphorescence, as a rule, with millisecond lifetimes, has been abundantly reported for some Pb(II) coordination polymers,[91] constructed mainly from aromatic carboxylate blocks.[92−96] Alternatively, efficient room-temperature phosphorescence of organic components has been realized in lead perovskites by introducing chromophore cations[29,97,98] or sensitizing agents.[99] However, on a molecular scale, complex **3** is one of the so far very few molecular lead compounds exhibiting phosphorescence at ambient temperature.[100,101]

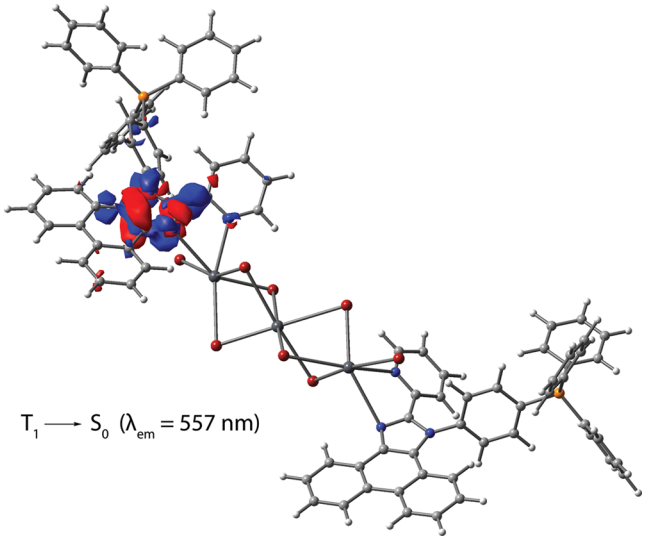

Figure 7. Electron density difference plot for the lowest energy triplet emission $T_1 \rightarrow S_0$ in complex **3** (isovalue 0.002 a.u., DFT-LRC-ωPBEh method using the CPCM solvation model[75] with toluene as a solvent, optimized T_1 geometry). During the electronic transition, the electron density increases in the red areas and decreases in the blue areas.

CONCLUSIONS

In this work, we have demonstrated the strategy of using the cationic diimine ligand, phosphonium-functionalized phenanthro-imidazolyl pyridine LP^+Br, for the straightforward preparation of inorganic−organic hybrid complexes of zinc (**1**), cadmium (**2**), and lead (**3**). Compounds **1** and **2** represent zero-dimensional salts containing ligand-derived complex cations $[LP^+MBr_2]^+$ and bromometalate anions $[MBr_4]^{2-}$. The lead bromide resulted in the assembly of a novel type of zwitterionic complex, in which the anionic cluster $[Pb_3Br_8]^{2-}$ is stabilized by two coordinated motifs LP^+. The analysis of the photophysical behavior of **1**–**3** in the solid state showed that the properties of **1** and **2** are governed by the intraligand charge transfer, resulting in moderate blue fluorescence, which is visibly enhanced versus the parent organic salt LP^+Br. On the other hand, complex **3** demonstrates a weak fluorescence signal along with room-temperature phosphorescence, which is a very rare case for Pb(II) molecular compounds. The phosphorescence mainly originates from an intraligand transition, while the lead and bromine atoms act as external heavy elements to boost the spin−orbit coupling. Notably, weak luminescence of crystalline **3** is drastically enhanced in the amorphous state, retaining the dominating role of the triplet excited state. Essentially, it allows ascribing the observed photoemission of **3** to the molecular properties but not to the consequence of crystal packing. Thus, it potentially opens ways for new structural chemistry and for tuning the optical characteristics of related hybrid and zwitterionic species by employing positively charged organic ligands possessing different chromophore fragments and a variable number of cationic groups. Despite presenting a case study of one particular ligand, the described concept likely can be applied to a large selection of organic ligands that will allow generation of novel ionic crystalline materials, zwitterionic aggregates, and heterometallic systems with rich photophysical behavior. Although **3** undergoes complete dissociation in solution, it is efficiently assembled upon solvent removal, which is presumably facilitated by the electrostatic attraction of inorganic and organic blocks. No less important is the stability of **3** toward water that enables convenient fabrication, handling, and solution processing of the complex without special precautions.

ASSOCIATED CONTENT

Supporting Information

The Supporting Information is available free of charge at https://pubs.acs.org/doi/10.1021/acs.inorgchem.2c02867.

Crystal data and structure refinement for **1**−**3**; selected structural parameters for **1**−**3**; and additional spectroscopic and computational data and figures (PDF)

Accession Codes

CCDC 2195808−2195810 contain the supplementary crystallographic data for this paper. These data can be obtained free of charge via www.ccdc.cam.ac.uk/data_request/cif, or by emailing data_request@ccdc.cam.ac.uk, or by contacting The Cambridge Crystallographic Data Centre, 12 Union Road, Cambridge CB2 1EZ, UK; fax: +44 1223 336033.

CCDC 2119917-2119918 also contains the supplementary crystallographic data for this paper.

AUTHOR INFORMATION

Corresponding Authors

Antti J. Karttunen − *Department of Chemistry and Materials Science, Aalto University, Aalto 00076, Finland;* orcid.org/0000-0003-4187-5447; Email: antti.karttunen@aalto.fi

Pi-Tai Chou − *Department of Chemistry, National Taiwan University, Taipei 10617, Taiwan;* orcid.org/0000-0002-8925-7747; Email: chop@ntu.edu.tw

Igor O. Koshevoy − *Department of Chemistry, University of Eastern Finland, Joensuu 80101, Finland;* orcid.org/0000-0003-4380-1302; Email: igor.koshevoy@uef.fi

Authors

Diana Temerova − *Department of Chemistry, University of Eastern Finland, Joensuu 80101, Finland*

Tai-Che Chou − *Department of Chemistry, National Taiwan University, Taipei 10617, Taiwan*

Kristina S. Kisel − *Department of Chemistry, University of Eastern Finland, Joensuu 80101, Finland*

Toni Eskelinen − *Department of Chemistry and Materials Science, Aalto University, Aalto 00076, Finland*

Niko Kinnunen − *Department of Chemistry, University of Eastern Finland, Joensuu 80101, Finland;* orcid.org/0000-0002-2286-274X

Janne Jänis − *Department of Chemistry, University of Eastern Finland, Joensuu 80101, Finland;* orcid.org/0000-0002-8446-4704

Complete contact information is available at: https://pubs.acs.org/10.1021/acs.inorgchem.2c02867

Author Contributions

The manuscript was written through contributions of all authors. All authors have given approval to the final version of the manuscript.

Notes

The authors declare no competing financial interest.

■ ACKNOWLEDGMENTS

Financial support from the Academy of Finland (decision 317903, I.O.K.; decision 340584, T.E. and A.J.K.; Flagship Programme, Photonics Research and Innovation PREIN, decision 320166) and computational resources from the Finnish IT Center for Science (CSC) are gratefully acknowledged.

■ REFERENCES

(1) Parola, S.; Julián-López, B.; Carlos, L. D.; Sanchez, C. Optical Properties of Hybrid Organic-Inorganic Materials and their Applications. *Adv. Funct. Mater.* **2016**, *26*, 6506−6544.

(2) McCall, K. M.; Morad, V.; Benin, B. M.; Kovalenko, M. V. Efficient Lone-Pair-Driven Luminescence: Structure−Property Relationships in Emissive $5s^2$ Metal Halides. *ACS Mater. Lett.* **2020**, *2*, 1218−1232.

(3) Gao, R.; Kodaimati, M. S.; Yan, D. Recent advances in persistent luminescence based on molecular hybrid materials. *Chem. Soc. Rev.* **2021**, *50*, 5564−5589.

(4) Han, Y.; Yue, S.; Cui, B.-B. Low-Dimensional Metal Halide Perovskite Crystal Materials: Structure Strategies and Luminescence Applications. *Adv. Sci.* **2021**, *8*, No. 2004805.

(5) Ganose, A. M.; Savory, C. N.; Scanlon, D. O. Beyond methylammonium lead iodide: prospects for the emergent field of ns2 containing solar absorbers. *Chem. Commun.* **2017**, *53*, 20−44.

(6) Lin, H.; Zhou, C.; Tian, Y.; Siegrist, T.; Ma, B. Low-Dimensional Organometal Halide Perovskites. *ACS Energy Lett.* **2018**, *3*, 54−62.

(7) Kundu, J.; Das, D. K. Low Dimensional, Broadband, Luminescent Organic-Inorganic Hybrid Materials for Lighting Applications. *Eur. J. Inorg. Chem.* **2021**, *2021*, 4508−4520.

(8) Li, M.; Xia, Z. Recent progress of zero-dimensional luminescent metal halides. *Chem. Soc. Rev.* **2021**, *50*, 2626−2662.

(9) Zhou, C.; Xu, L.-J.; Lee, S.; Lin, H.; Ma, B. Recent Advances in Luminescent Zero-Dimensional Organic Metal Halide Hybrids. *Adv. Opt. Mater.* **2021**, *9*, No. 2001766.

(10) Zhou, L.; Liao, J.-F.; Kuang, D.-B. An Overview for Zero-Dimensional Broadband Emissive Metal-Halide Single Crystals. *Adv. Opt. Mater.* **2021**, *9*, No. 2100544.

(11) Sun, S.; Lu, M.; Gao, X.; Shi, Z.; Bai, X.; Yu, W. W.; Zhang, Y. 0D Perovskites: Unique Properties, Synthesis, and Their Applications. *Adv. Sci.* **2021**, *8*, No. 2102689.

(12) Zhou, C.; Worku, M.; Neu, J.; Lin, H.; Tian, Y.; Lee, S.; Zhou, Y.; Han, D.; Chen, S.; Hao, A.; Djurovich, P. I.; Siegrist, T.; Du, M.-H.; Ma, B. Facile Preparation of Light Emitting Organic Metal Halide Crystals with Near-Unity Quantum Efficiency. *Chem. Mater.* **2018**, *30*, 2374−2378.

(13) Yangui, A.; Roccanova, R.; McWhorter, T. M.; Wu, Y.; Du, M.-H.; Saparov, B. Hybrid Organic−Inorganic Halides $(C_5H_7N_2)_2MBr_4$ (M = Hg, Zn) with High Color Rendering Index and High-Efficiency White-Light Emission. *Chem. Mater.* **2019**, *31*, 2983−2991.

(14) Li, Q.; Chen, Z.; Li, M.; Xu, B.; Han, J.; Luo, Z.; Tan, L.; Xia, Z.; Quan, Z. Pressure-Engineered Photoluminescence Tuning in Zero-Dimensional Lead Bromide Trimer Clusters. *Angew. Chem., Int. Ed.* **2021**, *60*, 2583−2587.

(15) Morad, V.; Yakunin, S.; Benin, B. M.; Shynkarenko, Y.; Grotevent, M. J.; Shorubalko, I.; Boehme, S. C.; Kovalenko, M. V. Hybrid 0D Antimony Halides as Air-Stable Luminophores for High-Spatial-Resolution Remote Thermography. *Adv. Mater.* **2021**, *33*, No. 2007355.

(16) Qi, Z.; Chen, Y.; Guo, Y.; Yang, X.; Zhang, F.-Q.; Zhou, G.; Zhang, X.-M. Broadband white-light emission in a one-dimensional organic−inorganic hybrid cadmium chloride with face-sharing CdCl6 octahedral chains. *J. Mater. Chem. C* **2021**, *9*, 88−94.

(17) Wei, J.-H.; Liao, J.-F.; Zhou, L.; Luo, J.-B.; Wang, X.-D.; Kuang, D.-B. Indium-antimony-halide single crystals for high-efficiency white-light emission and anti-counterfeiting. *Sci. Adv.* **2021**, *7*, No. eabg3989.

(18) Feng, S.; Ma, Y.; Wang, S.; Gao, S.; Huang, Q.; Zhen, H.; Yan, D.; Ling, Q.; Lin, Z. Light/Force-Sensitive 0D Lead-Free Perovskites: From Highly Efficient Blue Afterglow to White Phosphorescence with Near-Unity Quantum Efficiency. *Angew. Chem., Int. Ed.* **2022**, *61*, No. e202116511.

(19) Barkaoui, H.; Abid, H.; Yangui, A.; Triki, S.; Boukheddaden, K.; Abid, Y. Yellowish White-Light Emission Involving Resonant Energy Transfer in a New One-Dimensional Hybrid Material: $(C_9H_{10}N_2)$-$PbCl_4$. *J. Phys. Chem. C* **2018**, *122*, 24253−24261.

(20) Roccanova, R.; Houck, M.; Yangui, A.; Han, D.; Shi, H.; Wu, Y.; Glatzhofer, D. T.; Powell, D. R.; Chen, S.; Fourati, H.; Lusson, A.; Boukheddaden, K.; Du, M.-H.; Saparov, B. Broadband Emission in Hybrid Organic−Inorganic Halides of Group 12 Metals. *ACS Omega* **2018**, *3*, 18791−18802.

(21) Li, K.-J.; Zhao, Y.-Y.; Sun, M.-E.; Chen, G.-S.; Zhang, C.; Liu, H.-L.; Li, H.-Y.; Zang, S.-Q.; Mak, T. C. W. Zero-Dimensional Zinc Halide Organic Hybrids with Excellent Optical Waveguide Properties. *Cryst. Growth Des.* **2022**, *22*, 3295−3302.

(22) McWhorter, T. M.; Zhang, Z.; Creason, T. D.; Thomas, L.; Du, M.-H.; Saparov, B. (C7H11N2)2MBr4 (M=Cu, Zn): X-Ray Sensitive 0D Hybrid Metal Halides with Tunable Broadband Emission. *Eur. J. Inorg. Chem.* **2022**, *2022*, No. e202100954.

(23) Fattal, H.; Creason, T. D.; Delzer, C. J.; Yangui, A.; Hayward, J. P.; Ross, B. J.; Du, M.-H.; Glatzhofer, D. T.; Saparov, B. Zero-Dimensional Hybrid Organic−Inorganic Indium Bromide with Blue Emission. *Inorg. Chem.* **2021**, *60*, 1045−1054.

(24) Yangui, A.; Roccanova, R.; Wu, Y.; Du, M.-H.; Saparov, B. Highly Efficient Broad-Band Luminescence Involving Organic and Inorganic Molecules in a Zero-Dimensional Hybrid Lead Chloride. *J. Phys. Chem. C* **2019**, *123*, 22470−22477.

(25) Zhang, W.-F.; Pan, W.-J.; Xu, T.; Song, R.-Y.; Zhao, Y.-Y.; Yue, C.-Y.; Lei, X.-W. One-Dimensional Face-Shared Perovskites with Broad-Band Bluish White-Light Emissions. *Inorg. Chem.* **2020**, *59*, 14085−14092.

(26) Dammak, T.; Abid, Y. Quasi-white light emission involving Förster resonance energy transfer in a new organic inorganic tin chloride based material (AMPS)[SnCl6]H2O. *Opt. Mater.* **2017**, *66*, 302−307.

(27) Sun, X.-Y.; Yue, M.; Jiang, Y.-X.; Zhao, C.-H.; Liao, Y.-Y.; Lei, X.-W.; Yue, C.-Y. Combining Dual-Light Emissions to Achieve

Efficient Broadband Yellowish-Green Luminescence in One-Dimensional Hybrid Lead Halides. *Inorg. Chem.* **2021**, *60*, 1491−1498.
(28) Huang, Q.; Yang, S.; Feng, S.; Zhen, H.; Lin, Z.; Ling, Q. Multicolor Output from 2D Hybrid Perovskites with Wide Band Gap: Highly Efficient White Emission, Dual-Color Afterglow, and Switch between Fluorescence and Phosphorescence. *J. Phys. Chem. Lett.* **2021**, *12*, 1040−1045.
(29) Chaaban, M.; Ben-Akacha, A.; Worku, M.; Lee, S.; Neu, J.; Lin, X.; Vellore Winfred, J. S. R.; Delzer, C. J.; Hayward, J. P.; Du, M.-H.; Siegrist, T.; Ma, B. Metal Halide Scaffolded Assemblies of Organic Molecules with Enhanced Emission and Room Temperature Phosphorescence. *J. Phys. Chem. Lett.* **2021**, *12*, 8229−8236.
(30) Xu, L.-J.; Plaviak, A.; Lin, X.; Worku, M.; He, Q.; Chaaban, M.; Kim, B. J.; Ma, B. Metal Halide Regulated Photophysical Tuning of Zero-Dimensional Organic Metal Halide Hybrids: From Efficient Phosphorescence to Ultralong Afterglow. *Angew. Chem., Int. Ed.* **2020**, *59*, 23067−23071.
(31) Liu, S.; Fang, X.; Lu, B.; Yan, D. Wide range zero-thermal-quenching ultralong phosphorescence from zero-dimensional metal halide hybrids. *Nat. Commun.* **2020**, *11*, No. 4649.
(32) Lee, L. C.-C.; Lo, K. K.-W. Luminescent and Photofunctional Transition Metal Complexes: From Molecular Design to Diagnostic and Therapeutic Applications. *J. Am. Chem. Soc.* **2022**, *144*, 14420−14440.
(33) Artem'ev, A. V.; Pritchina, E. A.; Rakhmanova, M. I.; Gritsan, N. P.; Bagryanskaya, I. Y.; Malysheva, S. F.; Belogorlova, N. A. Alkyl-dependent self-assembly of the first red-emitting zwitterionic {Cu4I6} clusters from [alkyl-P(2-Py)3]+ salts and CuI: when size matters. *Dalton Trans.* **2019**, *48*, 2328−2337.
(34) Zhu, K.; Cheng, Z.; Rangan, S.; Cotlet, M.; Du, J.; Kasaei, L.; Teat, S. J.; Liu, W.; Chen, Y.; Feldman, L. C.; O'Carroll, D. M.; Li, J. A New Type of Hybrid Copper Iodide as Nontoxic and Ultrastable LED Emissive Layer Material. *ACS Energy Lett.* **2021**, *6*, 2565−2574.
(35) Bazany-Rodríguez, I. J.; Salomón-Flores, M. K.; Viviano-Posadas, A. O.; García-Eleno, M. A.; Barroso-Flores, J.; Martínez-Otero, D.; Dorazco-González, A. Chemosensing of neurotransmitters with selectivity and naked eye detection of l-DOPA based on fluorescent Zn(ii)-terpyridine bearing boronic acid complexes. *Dalton Trans.* **2021**, *50*, 4255−4269.
(36) Kozhevnikov, D. N.; Shabunina, O. V.; Kopchuk, D. S.; Slepukhin, P. A.; Kozhevnikov, V. N. 5-Aryl-2,2′-bipyridines as tunable fluorophores. *Tetrahedron Lett.* **2006**, *47*, 7025−7029.
(37) Ardizzoia, G. A.; Brenna, S.; Durini, S.; Therrien, B.; Veronelli, M. Synthesis, Structure, and Photophysical Properties of Blue-Emitting Zinc(II) Complexes with 3-Aryl-Substituted 1-Pyridylimidazo[1,5-a]pyridine Ligands. *Eur. J. Inorg. Chem.* **2014**, *2014*, 4310−4319.
(38) Wang, X.-M.; Chen, S.; Fan, R.-Q.; Zhang, F.-Q.; Yang, Y.-L. Facile luminescent tuning of ZnII/HgII complexes based on flexible, semi-rigid and rigid polydentate Schiff bases from blue to green to red: structural, photophysics, electrochemistry and theoretical calculations studies. *Dalton Trans.* **2015**, *44*, 8107−8125.
(39) Dong, Y.; Fan, R.; Chen, W.; Wang, P.; Yang, Y. A simple quinolone Schiff-base containing CHEF based fluorescence 'turn-on' chemosensor for distinguishing Zn^{2+} and Hg^{2+} with high sensitivity, selectivity and reversibility. *Dalton Trans.* **2017**, *46*, 6769−6775.
(40) Tsukamoto, T.; Aoki, R.; Sakamoto, R.; Toyoda, R.; Shimada, M.; Hattori, Y.; Kitagawa, Y.; Nishibori, E.; Nakano, M.; Nishihara, H. Mechano-, thermo-, solvato-, and vapochromism in bis(acetato-κ^1O)[4′-(4-(diphenylamino)phenyl)](2,2′:6′,2″-terpyridine-κ^3N,N′,N″)zinc(ii) and its polymer. *Chem. Commun.* **2017**, *53*, 9805−9808.
(41) Hiscock, L. K.; Joekar, D.; Balonova, B.; Tomas Piqueras, M.; Schroeder, Z. W.; Jarvis, V.; Maly, K. E.; Blight, B. A.; Dawe, L. N. Structures, Phase Behavior, and Fluorescent Properties of 3-Phenyl-1-(pyridin-2-yl)-1H-pyrazol-5-amine and Its $ZnCl_2$ Complex. *Inorg. Chem.* **2019**, *58*, 16317−16321.
(42) Temerova, D.; Kisel, K. S.; Eskelinen, T.; Melnikov, A. S.; Kinnunen, N.; Hirva, P.; Shakirova, J. R.; Tunik, S. P.; Grachova, E. V.; Koshevoy, I. O. Diversifying the luminescence of phenanthro-diimine ligands in zinc complexes. *Inorg. Chem. Front.* **2021**, *8*, 2549−2560.
(43) Nugent, J. W.; Lee, H.; Lee, H.-S.; Reibenspies, J. H.; Hancock, R. D. Mechanism of chelation enhanced fluorescence in complexes of cadmium(ii), and a possible new type of anion sensor. *Chem. Commun.* **2013**, *49*, 9749−9751.
(44) Wang, Z.; Zhu, C.-Y.; Yin, S.-Y.; Wei, Z.-W.; Zhang, J.-H.; Fan, Y.-N.; Jiang, J.-J.; Pan, M.; Su, C.-Y. A Metal−Organic Supramolecular Box as a Universal Reservoir of UV, WL, and NIR Light for Long-Persistent Luminescence. *Angew. Chem., Int. Ed.* **2019**, *58*, 3481−3485.
(45) Liang, Q.-F.; Zheng, H.-W.; Yang, D.-D.; Zheng, X.-J. A triphenylamine derivative and its Cd(ii) complex with high-contrast mechanochromic luminescence and vapochromism. *CrystEngComm* **2022**, *24*, 543−551.
(46) Volpi, G.; Priola, E.; Garino, C.; Daolio, A.; Rabezzana, R.; Benzi, P.; Giordana, A.; Diana, E.; Gobetto, R. Blue fluorescent zinc(II) complexes based on tunable imidazo[1,5-a]pyridines. *Inorg. Chim. Acta* **2020**, *509*, No. 119662.
(47) Younes, A. H.; Zhang, L.; Clark, R. J.; Zhu, L. Fluorescence of 5-Arylvinyl-5′-Methyl-2,2′-Bipyridyl Ligands and Their Zinc Complexes. *J. Org. Chem.* **2009**, *74*, 8761−8772.
(48) Divya, K. P.; Sreejith, S.; Balakrishna, B.; Jayamurthy, P.; Anees, P.; Ajayaghosh, A. A Zn2+-specific fluorescent molecular probe for the selective detection of endogenous cyanide in biorelevant samples. *Chem. Commun.* **2010**, *46*, 6069−6071.
(49) Wang, Z.; Zhu, C.-Y.; Mo, J.-T.; Xu, X.-Y.; Ruan, J.; Pan, M.; Su, C.-Y. Multi-Mode Color-Tunable Long Persistent Luminescence in Single-Component Coordination Polymers. *Angew. Chem., Int. Ed.* **2021**, *60*, 2526−2533.
(50) Kozhevnikov, V. N.; Shabunina, O. V.; Kopchuk, D. S.; Ustinova, M. M.; König, B.; Kozhevnikov, D. N. Facile synthesis of 6-aryl-3-pyridyl-1,2,4-triazines as a key step toward highly fluorescent 5-substituted bipyridines and their Zn(II) and Ru(II) complexes. *Tetrahedron* **2008**, *64*, 8963−8973.
(51) Hao, P.; Liu, X.; Guo, C.; Zhao, G.; Li, G.; Shen, J.; Fu, Y. Lattice solvent controlled photochromism of tripyridyl-triazine-based zinc bromide complexes. *Inorg. Chem. Front.* **2022**, *9*, 879−888.
(52) Zhu, H.-G.; Xu, Y.; Yu, Z.; Wu, Q.-J.; Fun, H.-K.; You, X.-Z. The synthesis, structure of 1-D lead halide adducts: PbI2(L) (L = 2,2′-bipyridine, 1,10-phenanthroline). *Polyhedron* **1999**, *18*, 3491−3495.
(53) Marandi, F.; Garousi, E.; Fun, H.-K. Supramolecular organization in lead(II) halides of 4,4′-dimethoxy-2,2′-bipyridine ligand. *J. Mol. Struct.* **2013**, *1049*, 205−211.
(54) Travis, W.; Knapp, C. E.; Savory, C. N.; Ganose, A. M.; Kafourou, P.; Song, X.; Sharif, Z.; Cockcroft, J. K.; Scanlon, D. O.; Bronstein, H.; Palgrave, R. G. Hybrid Organic−Inorganic Coordination Complexes as Tunable Optical Response Materials. *Inorg. Chem.* **2016**, *55*, 3393−3400.
(55) Thompson, J. R.; Snider, D.; Wren, J. E. C.; Kroeker, S.; Williams, V. E.; Leznoff, D. B. Correlating Structural Features and 207Pb NMR Parameters with the Stereochemical Activity of PbII Lone Pairs in Birefringent Pb[2,6-bis(benzimidazol-2-yl)pyridine] Complexes. *Eur. J. Inorg. Chem.* **2017**, *2017*, 88−98.
(56) Yang, Y.; Wu, Y.; Mei, D.; Qu, Y. Lead-based crystal luminophores: Tuning emissive crystals and application for recording high temperature history with ratiometric and colorimetric signals. *Chem. Eng. J.* **2019**, *358*, 606−613.
(57) Qiu, K.; Ouyang, M.; Liu, Y.; Huang, H.; Liu, C.; Chen, Y.; Ji, L.; Chao, H. Two-photon photodynamic ablation of tumor cells by mitochondria-targeted iridium(III) complexes in aggregate states. *J. Mater. Chem. B* **2017**, *5*, 5488−5498.
(58) Kisel, K. S.; Eskelinen, T.; Zafar, W.; Solomatina, A. I.; Hirva, P.; Grachova, E. V.; Tunik, S. P.; Koshevoy, I. O. Chromophore-functionalized phenanthro-diimine ligands and their Re(I) complexes. *Inorg. Chem.* **2018**, *57*, 6349−6361.

https://doi.org/10.1021/acs.inorgchem.2c02867
Inorg. Chem. 2022, 61, 19220−19231

(59) Marcoux, D.; Charette, A. B. Palladium-Catalyzed Synthesis of Functionalized Tetraarylphosphonium Salts. *J. Org. Chem.* **2008**, *73*, 590−593.
(60) *APEX2 - Software Suite for Crystallographic Programs*; Bruker AXS, Inc: Madison, WI, USA, 2010.
(61) Sheldrick, G. M. *SADABS-2008/1 - Bruker AXS Area Detector Scaling and Absorption Correction*; Bruker AXS: Madison, Wisconsin, USA, 2008.
(62) Sheldrick, G. M. Crystal structure refinement with SHELXL. *Acta Crystallogr., Sect. C: Struct. Chem.* **2015**, *71*, 3−8.
(63) Farrugia, L. J. WinGX and ORTEP for Windows: an Update. *J. Appl. Crystallogr.* **2012**, *45*, 849−854.
(64) Spek, A. L. PLATON SQUEEZE: a tool for the calculation of the disordered solvent contribution to the calculated structure factors. *Acta Crystallogr., Sect. C: Struct. Chem.* **2015**, *71*, 9−18.
(65) Spek, A. L. *PLATON, A Multipurpose Crystallographic Tool*; Utrecht University: Utrecht, The Netherlands, 2001.
(66) Perdew, J. P.; Burke, K.; Ernzerhof, M. Generalized Gradient Approximation Made Simple. *Phys. Rev. Lett.* **1996**, *77*, 3865−3868.
(67) Adamo, C.; Barone, V. Toward reliable density functional methods without adjustable parameters: The PBE0 model. *J. Chem. Phys.* **1999**, *110*, 6158−6170.
(68) Weigend, F.; Ahlrichs, R. Balanced Basis Sets of Split Valence, Triple Zeta Valence and Quadruple Zeta Valence Quality for H to Rn: Design and Assessment of Accuracy. *Phys. Chem. Chem. Phys.* **2005**, *7*, 3297−3305.
(69) Andrae, D.; Häußermann, U.; Dolg, M.; Stoll, H.; Preuß, H. Energy-Adjusted Ab Initio Pseudopotentials for the Second and Third Row Transition Elements. *Theor. Chem. Acta.* **1990**, *77*, 123−141.
(70) Dapprich, S.; Komáromi, I.; Byun, K. S.; Morokuma, K.; Frisch, M. J. A new ONIOM implementation in Gaussian98. Part I. The calculation of energies, gradients, vibrational frequencies and electric field derivatives. *J. Mol. Struct.: THEOCHEM* **1999**, *461-462*, 1−21.
(71) Rappe, A. K.; Casewit, C. J.; Colwell, K. S.; Goddard, W. A.; Skiff, W. M. UFF, a full periodic table force field for molecular mechanics and molecular dynamics simulations. *J. Am. Chem. Soc.* **1992**, *114*, 10024−10035.
(72) Rappe, A. K.; Goddard, W. A. Charge equilibration for molecular dynamics simulations. *J. Phys. Chem. A* **1991**, *95*, 3358−3363.
(73) Frisch, M. J.; Trucks, G. W.; Schlegel, H. B.; Scuseria, G. E.; Robb, M. A.; Cheeseman, J. R.; Scalmani, G.; Barone, V.; Petersson, G. A.; Nakatsuji, H.; Li, X.; Caricato, M.; Marenich, A. V.; Bloino, J.; Janesko, B. G.; Gomperts, R.; Mennucci, B.; Hratchian, H. P.; Ortiz, J. V.; Izmaylov, A. F.; Sonnenberg, J. L.; Williams; Ding, F.; Lipparini, F.; Egidi, F.; Goings, J.; Peng, B.; Petrone, A.; Henderson, T.; Ranasinghe, D.; Zakrzewski, V. G.; Gao, J.; Rega, N.; Zheng, G.; Liang, W.; Hada, M.; Ehara, M.; Toyota, K.; Fukuda, R.; Hasegawa, J.; Ishida, M.; Nakajima, T.; Honda, Y.; Kitao, O.; Nakai, H.; Vreven, T.; Throssell, K.; Montgomery, J. A., Jr.; Peralta, J. E.; Ogliaro, F.; Bearpark, M. J.; Heyd, J. J.; Brothers, E. N.; Kudin, K. N.; Staroverov, V. N.; Keith, T. A.; Kobayashi, R.; Normand, J.; Raghavachari, K.; Rendell, A. P.; Burant, J. C.; Iyengar, S. S.; Tomasi, J.; Cossi, M.; Millam, J. M.; Klene, M.; Adamo, C.; Cammi, R.; Ochterski, J. W.; Martin, R. L.; Morokuma, K.; Farkas, O.; Foresman, J. B.; Fox, D. J. *Gaussian 16*, Rev. C.01, Wallingford, CT 2016.
(74) Neese, F. Software update: The ORCA program system-Version 5.0. *WIREs Comput. Mol. Sci.* **2022**, *12*, No. e1606.
(75) Barone, V.; Cossi, M. Quantum Calculation of Molecular Energies and Energy Gradients in Solution by a Conductor Solvent Model. *J. Phys. Chem. A* **1998**, *102*, 1995−2001.
(76) Rohrdanz, M. A.; Martins, K. M.; Herbert, J. M. A long-range-corrected density functional that performs well for both ground-state properties and time-dependent density functional theory excitation energies, including charge-transfer excited states. *J. Chem. Phys.* **2009**, *130*, No. 054112.
(77) Neese, F. An improvement of the resolution of the identity approximation for the formation of the Coulomb matrix. *J. Comput. Chem.* **2003**, *24*, 1740−1747.
(78) Neese, F.; Wennmohs, F.; Hansen, A.; Becker, U. Efficient, approximate and parallel Hartree−Fock and hybrid DFT calculations. A 'chain-of-spheres' algorithm for the Hartree−Fock exchange. *Chem. Phys.* **2009**, *356*, 98−109.
(79) Chen, S.; Fan, R.-Q.; Wang, X.-M.; Yang, Y.-L. Novel bright blue emissions IIB group complexes constructed with various polyhedron-induced 2-[2′-(6-methoxy-pyridyl)]-benzimidazole derivatives. *CrystEngComm* **2014**, *16*, 6114−6125.
(80) Song, Y.; Kim, D.; Lee, H.-J.; Lee, H. Cd(II) and Zn(II) Complexes Containing N,N'-Bidentate N-(Pyridin-2-ylmethylene)-cyclopentanamine: Synthesis, Characterisation and Methyl Methacrylate Polymerisation. *Bull. Korean Chem. Soc.* **2014**, *35*, 2929−2934.
(81) Kokina, T. E.; Glinskaya, L. A.; Tkachev, A. V.; Plyusnin, V. F.; Tsoy, Y. V.; Bagryanskaya, I. Y.; Vasilyev, E. S.; Piryazev, D. A.; Sheludyakova, L. A.; Larionov, S. V. Chiral zinc(II) and cadmium(II) complexes with a dihydrophenanthroline ligand bearing (−)-α-pinene fragments: Synthesis, crystal structures and photophysical properties. *Polyhedron* **2016**, *117*, 437−444.
(82) Munshi, S. J.; Saini, J. K.; Ingle, S.; Kumar, S. B. Metal(II) chloride complexes containing a tridentate N-donor Schiff base ligand: syntheses, structures and antimicrobial activity. *J. Coord. Chem.* **2021**, *74*, 2004−2016.
(83) Klapötke, T. M.; Krumm, B.; Polbom, K.; Rienäcker, C. M. Synthesis and Characterization of Bromo- and Bromochloroplumbates(II). Crystal Structures of $[Ph_4E]2[Pb_3Br_8]$ (E = P, As) and $[Ph_4P][PbBrCl_2] \bullet CH_3CN$. *Z. Naturforsch. B* **2000**, *55*, 377−382.
(84) Gröger, H.; Lode, C.; Vollmer, H.; Krautscheid, H.; Lebedkin, S. Bromoplumbate mit kettenförmigen und isolierten Anionen: $(Bzl_4P)_2[Pb_3Br_8]$, $(Bzl_4P)_2[Pb_3Br_8(dmf)_2]$, $(Bzl_4P)[PbBr_3]$, $(Bzl_4P)_2[PbBr_4]$ und $(Bzl_4P)_4[Pb_2Br_6][PbBr_4]$. *Z. Anorg. Allg. Chem.* **2002**, *628*, 57−62.
(85) Morad, V.; Shynkarenko, Y.; Yakunin, S.; Brumberg, A.; Schaller, R. D.; Kovalenko, M. V. Disphenoidal Zero-Dimensional Lead, Tin, and Germanium Halides: Highly Emissive Singlet and Triplet Self-Trapped Excitons and X-ray Scintillation. *J. Am. Chem. Soc.* **2019**, *141*, 9764−9768.
(86) Lin, H.; Zhou, C.; Chaaban, M.; Xu, L.-J.; Zhou, Y.; Neu, J.; Worku, M.; Berkwits, E.; He, Q.; Lee, S.; Lin, X.; Siegrist, T.; Du, M.-H.; Ma, B. Bulk Assembly of Zero-Dimensional Organic Lead Bromide Hybrid with Efficient Blue Emission. *ACS Mater. Lett.* **2019**, *1*, 594−598.
(87) Zhou, J.; Li, M.; Ning, L.; Zhang, R.; Molokeev, M. S.; Zhao, J.; Yang, S.; Han, K.; Xia, Z. Broad-Band Emission in a Zero-Dimensional Hybrid Organic $[PbBr_6]$ Trimer with Intrinsic Vacancies. *J. Phys. Chem. Lett.* **2019**, *10*, 1337−1341.
(88) Febriansyah, B.; Neo, C. S. D.; Giovanni, D.; Srivastava, S.; Lekina, Y.; Koh, T. M.; Li, Y.; Shen, Z. X.; Asta, M.; Sum, T. C.; Mathews, N.; England, J. Targeted Synthesis of Trimeric Organic−Bromoplumbate Hybrids That Display Intrinsic, Highly Stokes-Shifted, Broadband Emission. *Chem. Mater.* **2020**, *32*, 4431−4441.
(89) Reger, D. L.; Huff, M. F.; Rheingold, A. L.; Haggerty, B. S. Control of structure in lead(II) complexes using poly(pyrazolyl)-borate ligands. Stereochemically inactive lone pair in octahedral [HB(3,5-Me2pz)3]2Pb (pz = pyrazolyl ring). *J. Am. Chem. Soc.* **1992**, *114*, 579−584.
(90) Zhou, C.; Lin, H.; Neu, J.; Zhou, Y.; Chaaban, M.; Lee, S.; Worku, M.; Chen, B.; Clark, R.; Cheng, W.; Guan, J.; Djurovich, P.; Zhang, D.; Lü, X.; Bullock, J.; Pak, C.; Shatruk, M.; Du, M.-H.; Siegrist, T.; Ma, B. Green Emitting Single-Crystalline Bulk Assembly of Metal Halide Clusters with Near-Unity Photoluminescence Quantum Efficiency. *ACS Energy Lett.* **2019**, *4*, 1579−1583.
(91) Toma, O.; Mercier, N.; Allain, M.; Meinardi, F.; Botta, C. Lead(II) 4,4′-Bipyridine N-Oxide Coordination Polymers − Highly Phosphorescent Materials with Mechanochromic Luminescence Properties. *Eur. J. Inorg. Chem.* **2017**, *2017*, 844−850.
(92) Martínez-Casado, F. J.; Ramos-Riesco, M.; Rodríguez-Cheda, J. A.; Cucinotta, F.; Fernández-Martínez, A.; Garrido, L.; Matesanz, E.; Marchese, L. Short lead(ii) soaps: from weakly fluorescent crystals to

https://doi.org/10.1021/acs.inorgchem.2c02867
Inorg. Chem. 2022, 61, 19220−19231

strongly phosphorescent and structurally varied vitreous phases. A thermal, structural and spectroscopic study. *J. Mater. Chem. C* **2014**, *2*, 9489−9496.
(93) Liu, X.; Zhai, L.; Zhang, W.-W.; Zuo, J.-L.; Yang, Z.-X.; Ren, X.-M. Intense greenish phosphorescence emission under ambient conditions in a two-dimensional lead(ii) coordination polymer with a 1,1′-ethynebenzene-3,3′,5,5′-tetracarboxylate ligand. *Dalton Trans.* **2017**, *46*, 7953−7959.
(94) Wu, X.-S.; Wang, Y.-X.; Li, S.-Q.; Qian, Y.; Zhai, L.; Wang, X.-Z.; Ren, X.-M. Metal ion coordination enhancing quantum efficiency of ligand phosphorescence in a double-stranded helical chain coordination polymer of Pb2+ with nicotinic acid. *Dalton Trans.* **2018**, *47*, 14636−14643.
(95) Gao, X.-S.; Dai, H.-J.; Ding, M.-J.; Pei, W.-B.; Ren, X.-M. Stereochemically Active and Inactive Lone Pairs in Two Room-Temperature Phosphorescence Coordination Polymers of Pb2+ with Different Tricarboxylic Acids. *Inorg. Chem.* **2019**, *58*, 6772−6780.
(96) Zhu, L.-L.; Huang, Y.-E.; Gong, L.-K.; Huang, X.-Y.; Qi, X.-H.; Wu, X.-H.; Du, K.-Z. Ligand Control of Room-Temperature Phosphorescence Violating Kasha's Rule in Hybrid Organic−Inorganic Metal Halides. *Chem. Mater.* **2020**, *32*, 1454−1460.
(97) Hu, H.; Meier, F.; Zhao, D.; Abe, Y.; Gao, Y.; Chen, B.; Salim, T.; Chia, E. E. M.; Qiao, X.; Deibel, C.; Lam, Y. M. Efficient Room-Temperature Phosphorescence from Organic−Inorganic Hybrid Perovskites by Molecular Engineering. *Adv. Mater.* **2018**, *30*, No. 1707621.
(98) Yang, S.; Wu, D.; Gong, W.; Huang, Q.; Zhen, H.; Ling, Q.; Lin, Z. Highly efficient room-temperature phosphorescence and afterglow luminescence from common organic fluorophores in 2D hybrid perovskites. *Chem. Sci.* **2018**, *9*, 8975−8981.
(99) Gong, L.-K.; Li, J.-R.; Wu, Z.-F.; Hu, B.; Wang, Z.-P.; Shen, N.-N.; Hu, Q.-Q.; Deng, Z.-H.; Zhang, Z.-Z.; Fu, J.-J.; Du, K.-Z.; Huang, X.-Y. Enhancing the phosphorescence of hybrid metal halides through molecular sensitization. *J. Mater. Chem. C* **2019**, *7*, 9803−9807.
(100) Strasser, A.; Vogler, A. Intraligand phosphorescence of lead(II) *β*-diketonates under ambient conditions. *J. Photochem. Photobiol. A: Chem.* **2004**, *165*, 115−118.
(101) Strasser, A.; Vogler, A. Optical properties of thallium(I), lead(II) and bismuth(III) hexafluoroacetylacetonates. Intraligand phosphorescence under ambient conditions. *Inorg. Chem. Commun.* **2004**, *7*, 528−530.

https://doi.org/10.1021/acs.inorgchem.2c02867
Inorg. Chem. 2022, 61, 19220−19231